Through-Wall Propagation Effects on Doppler-Enhanced Frontal Radar Images of Humans

Shobha Sundar Ram and Angshul Majumdar
Indraprastha Institute of Information Technology, Delhi
New Delhi, India 110020
Email: shobha@iiitd.ac.in, angshul@iiitd.ac.in

***Abstract*— High-resolution frontal radar images of humans can be generated in free space conditions with a Doppler radar with a large radar aperture. Compressed sensing based two dimensional beamforming enables imaging of humans with sub-Nyquist number of elements in the radar aperture. In this work, we apply this imaging technique to humans in through-wall scenarios in indoor environments. Walls are complex propagation environments that introduce refraction, attenuation, ringing and multipath to the radar signal. In this work, we quantitatively analyze the impact of inhomogeneous walls on the direction-of-arrival estimation with array processing. Next, we examine the impact of wall clutter on compressed sensing based radar imaging. The radar data scattered by humans moving behind walls is simulated by hybridizing wall propagation models, derived through computational electromagnetic techniques, and electromagnetic primitive based models of moving humans.**

***Index Terms*— micro-Doppler, radar imaging, compressed sensing, FDTD**

I. Introduction

Over the last decade, radars have emerged as a promising technology for detecting the presence of humans behind walls since radar signals below X band frequencies can penetrate most building materials [1]–[8]. However, unlike camera images that convey a lot of information regarding human activities, radar signatures of humans are non-intuitive and difficult to interpret by untrained operators. Most through-wall radars generate top-view (range and cross-range) images of humans using wideband waveforms and large radar apertures [9]. However, a top-view image conveys limited information regarding human activity. A human is usually narrow along the down-range dimension and larger along the cross range dimensions. Therefore, the more natural and informative viewing perspective of a human is the frontal view (which closely imitates our human perception of other humans). Very large planar apertures operating at high carrier frequencies are required in order to generate frontal images of sufficiently high resolution [10]. However, high carrier frequencies are heavily attenuated by building materials. Also, large apertures with lots of array elements are complex and costly to build. Alternately, large apertures can be realized through synthetic aperture (SAR) techniques. But humans are rarely still. Therefore, sophisticated motion compensation techniques have to be implemented to remove the distortions introduced by human motions on SAR images [8].

In [11], we proposed a technique to generate high resolution Doppler-enhanced frontal images of humans with a Doppler radar of moderate complexity. It is well known that the scattered returns from moving humans yield micro-Dopplers that arise from the dynamic movements of different body parts. Our technique is based on resolving multiple point scatterers on the human along three dimensions - Doppler, azimuth and elevation. The additional Doppler dimension enables us to reduce the carrier frequency and aperture size required to resolve the different scatterers along the azimuth and elevation dimensions. Array processing along the cross-range dimensions is carried out by incorporating compressed sensing (CS) principles into two-dimensional beamforming. CS enables us to reduce the number of antenna elements below the Nyquist limits without altering the aperture size. CS has recently been widely adopted by the radar community for wideband SAR [12]–[22], through-wall and other remote sensing radars [23], [24], and MIMO radars [25], [26]. CS was particularly suited to our problem for two reasons: One, there is significant sparsity inherent in the radar image of a human when the radar aperture is large; second, two-dimensional beamforming via Fourier processing is a linear imaging process that lends itself to a variety of CS based algorithms.

The previous work was restricted to imaging humans in free space conditions. However, walls are complex propagation mediums that introduce refraction, attenuation, ringing and multipath to radar signals. There are two objectives of this paper - First, to measure the error introduced by complex walls on angle-of-arrival estimation through array processing; Second, to measure the robustness of the compressed sensing based radar imaging methodology, presented in [11], to through-wall propagation effects. We focus on two types of walls - a multilayer brick wall and an inhomogeneous concrete wall with metal reinforcements. The radar data of humans moving behind walls are simulated through electromagnetic primitive based models of humans combined with through-wall propagation models generated through finite difference time domain techniques. Then, the radar images of humans are generated through Doppler processing and CS based array processing.

This paper is organized as follows. In section II, we briefly describe the methodology for simulating wall propagation effects. In section III, we analyze the impact of multipath introduced by walls on direction-of-arrival estimation by one-dimensional array processing. Finally, in section IV, we present Doppler-enhanced frontal radar images of humans moving behind walls using CS based radar imaging. We,

978-1-5090-0863-6/16/$31.00 ©2016 IEEE

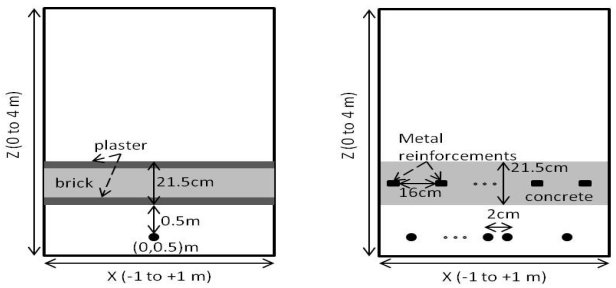

Fig. 1. FDTD simulations of (a) multilayered brick wall and (b) concrete with periodic metal (steel) reinforcements.

TABLE I
WALL PARAMETERS

Material	Thickness (cm)	Conductivity (Sm^{-1})	Dielectric Constant
Plaster	1.25	0.02	6
Brick	19	0.0349	4
Concrete	21.5	0.0245	7
Steel	1	7×10^6	

qualitatively and quantitatively, analyze the error introduced by through-wall phenomenology on the radar images.

II. Simulation of Through-Wall Propagation

We proposed a method to simulate complex through-wall propagation, in [27], using finite difference time domain (FDTD) simulations for a radar with a single transceiver element. In this work, we extend the method to simulate narrowband scattered returns on a radar with a single transmitter and a multiple element planar receiver array. We consider a $2m \times 4m$ two-dimensional space in the $X - Z$ Cartesian space as shown in Fig.1. A sinusoidal source of $7.5GHz$ is placed at position $[0, 0.5]m$. Berenger's perfectly matched layer (PML) of 12.5cm thickness is used for boundary conditions [28]. Two through-wall propagation cases are considered - First, we consider a multilayered wall, of 21.5cm thickness, consisting of a brick layer between two layers of plaster as shown in Fig.1(a); Second, we consider an inhomogeneous concrete wall of 21.5cm thickness with periodic square metal reinforcements, 16cm apart, along the X axis as shown in Fig.1(b). The thickness (along the Z dimension), dielectric constant and conductivity of the different wall materials are presented in Table.I. We assume that the simulation space is uniform along the Y axis in both the cases. The time domain simulations are carried out long enough (66ns) to reach steady state conditions. The FDTD grid size is 0.2cm and the time step is 3.25ps. The time-domain results for every point in space are Fourier transformed to obtain the propagation at 7.5GHz. For comparison purposes, we also simulate propagation in free space conditions using ray theory.

Fig.2 show the magnitude and phase response for the two cases for a region within the simulation space $[X : -0.6$ to $+0.6m, Z : 2.5m$ to $4m]$. We are restricting the study to this region since the human motions, considered in later sections, are assumed to be confined within this region. In free space (figure is not shown), the signal strength decreases as the distance from the source increases and the phase response shows circular wave propagation. The brick wall, in Fig.2(a), introduces a one-way propagation loss of approximately $10dB$. We also observe some artifacts due to limitations of the performance of the PML. However, this wall does not significantly distort the circular phase front of the propagating wave (Fig.2(c)). The concrete wall, with metal reinforcements, attenuates the propagation signal and also introduces significant multipath components that distort the magnitude and phase response as observed in Figs.2(b) and 2(d). There is considerable constructive and destructive interference between the multipath components at specific regions of the simulation space.

III. Wall Effects on DOA Estimation Using Array Processing

We use the FDTD results to gauge the accuracy of direction-of-arrival (DOA) estimation with linear array processing in through-wall scenarios. The DOA of a rigid target, in the far-field with respect to a linear antenna array of a radar, can be estimated through one dimensional Fourier processing of the radar returns. Consider a transmitter at $[x = 0, z = 0.5m]$ and a uniform linear receiver array, centered at $[x = 0, z = 0.5m]$, that consists of 20 transceiver elements along the X axis. The returns at each element of the array, from a single point target at $[x, z]$ in free space, are given by, $a(n) = e^{\frac{-j2\pi f_c r_n}{c}}$, where f_c is the propagation frequency, c is the speed of light and r_n is the radial distance of a target from the n^{th} antenna element. The DOA information of the target is obtained by Fourier processing of the radar data, with respect to the angle of arrival as shown in (1).

$$A(\theta) = \frac{1}{20} \sum_{n=1}^{20} a(n) e^{\frac{+j2\pi f_c d(n-1) sin\theta}{c}} \quad (1)$$

Here, d, is half the wavelength corresponding to the propagation frequency. $A(\theta)$ will peak at 1 at $\theta = DOA$ of the target. This is violated under two conditions: One, the target is in the near field of the antenna array; Two, there are multipath components between the target and the antenna array. Therefore, the deviation of $max|A(\theta)|$ from 1 is a useful indicator for the accuracy of DOA estimation using linear array processing.

Fig.4(a) shows $max|A(\theta)|$ for every possible position of a point target in the Cartesian space: $[X : -0.6m$ to $+0.6m$, $Z : 2.5m$ to $4m]$ for free space conditions. The figure shows that $A(\theta)$ peaks closer to 1 farther away from the antenna array. Nearer the antenna array, the phase information from the target is distorted due to near field effects which results in errors in array processing. We repeat the study on FDTD data at 7.5GHz. First, we consider the multilayered brick wall case. The problem space is homogeneous along the X axis. Consider a point target, tgt, at a position $[x, z]$ and a receiver element of the linear array at position $[0 \pm (n-1)d, 0.5]m$ as shown in Fig.3. The propagation path between tgt and

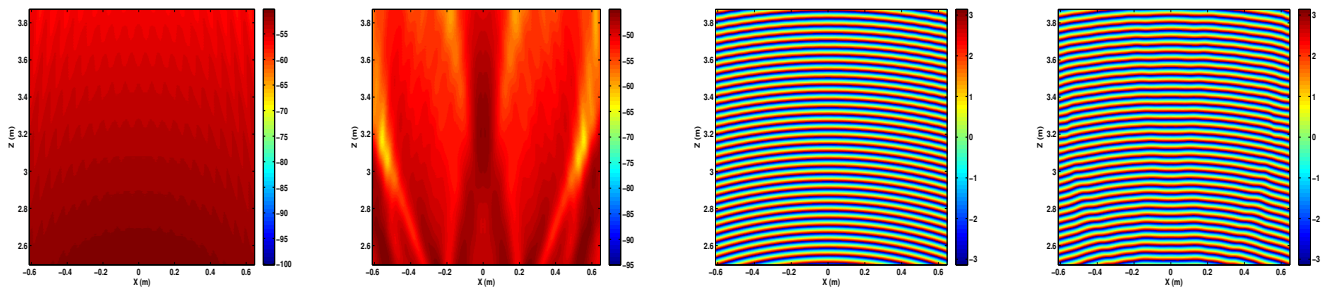

(a) (b) (c) (d)

Fig. 2. Magnitude response at 7.5GHz derived from FDTD simulations for (a) multilayered brick wall and (b) reinforced concrete. Phase response at 7.5GHz for (c) multilayered brick wall and (d) reinforced concrete wall.

the n^{th} antenna element is equivalent to the propagation path between a point scatterer at tgt' at $[x \mp (n-1)d, z]$ and the antenna element at $[0, 0.5]m$. Therefore, the radar

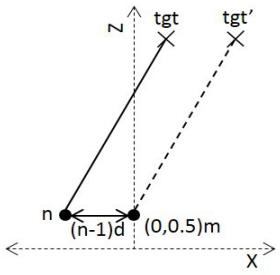

Fig. 3. Two-way propagation path between tgt and n^{th} antenna element is equivalent to square of frequency response of FDTD results at tgt' with respect to source

data at the n^{th} antenna element, $a(n)$, is equivalent to the frequency domain response of the FDTD data at tgt' since the source of the FDTD simulation is located at $[0, 0.5]m$. In order to remove the impact of the amplitude variation across the antenna elements, the radar returns at each element are scaled so as to have unity magnitude. $max|A(\theta)|$ is computed for every point in the Cartesian space, specified earlier, using (1) and shown in Fig.4(b). This wall introduces attenuation and ringing of the propagating wave. However, the DOA estimation is only slightly distorted when compared to the free space case. Finally, we consider the inhomogeneous concrete wall with the metal reinforcements. Due to the inhomogeneity in the problem space, FDTD simulations are carried out to determine $a(n)$ at every antenna element for all possible point target positions. The array processing results are presented in Fig.4(c). Due to the complex propagation channel, the array processing results are significantly distorted. Interference between the multipath components have significantly impacted the phase data and hence $A(\theta)$ has multiple peaks. Therefore, $max|A(\theta)|$ deviates further away from unity. This indicates that it may become challenging to correctly estimate the DOA under these circumstances.

IV. Doppler-Enhanced Frontal Radar Imaging Using Compressed Sensing

In this section, we examine the effects of through-wall propagation on frontal radar imaging of humans. Consider a human moving behind a wall before a Doppler radar, operating at 7.5GHz, with single transmitter and a uniform planar antenna array as shown in Fig.5. The planar array consists of $[N \times N]$ elements and lies in the $z = 0.5m$ plane centered at $[0, 1, 0.5]m$ which is also the position of the transmitter. The spacing between consecutive elements of the array is half-wavelength along both the X and Y axes. The wall is assumed to be uniform along the Y axis and 21.5cm thick along the Z axis. We consider two types of walls - the multilayered brick wall and the concrete wall with periodic metal reinforcements, that were described in the previous section. We simulate the radar returns scattered by a human behind the wall by combining electromagnetic primitive based modeling of the human with the FDTD simulations of through-wall propagation. We consider a human walking motion which is confined within the FDTD simulation space $[X : -0.6m$ to $+0.6m$, $Z : 2.5m$ to $4m]$. The electromagnetic model of the human consists of multiple point scatterers on primitives corresponding to different body parts. The radar returns consist of two-way propagation from the transmitter to the point scatterer at $[x, y, z]$ and the scattered returns back the receiver antenna element at $[0 \pm (n-1)d, 1 \pm (n-1)d, 0.5]m$. In the case of the brick wall, this propagation is modeled by the product of the FDTD frequency domain responses at $[x, z]$ and $[x \mp (n-d), z]$ for 7.5GHz. In the case of the concrete wall, individual FDTD simulations are carried out for each position of the antenna elements of the planar array along the X axis. The magnitude and phase of the two-dimensional FDTD data are appropriately calibrated to account for the three-dimensional positions of the point scatterers and the antenna elements. The propagation data for each point scatterer is combined with the radar cross-section of the corresponding primitive. The radar returns of the human are generated from the complex sum of the returns from all the primitives. This procedure is described in fuller detail in [27]. In order to qualitatively study the through-wall propagation effects, we also consider the human moving in free space. We generate ground truth data by modeling the propagation between a point scatterer and an antenna element of the planar array as $\frac{1}{r_1 r_2} e^{-jk(r_1+r_2)}$ where

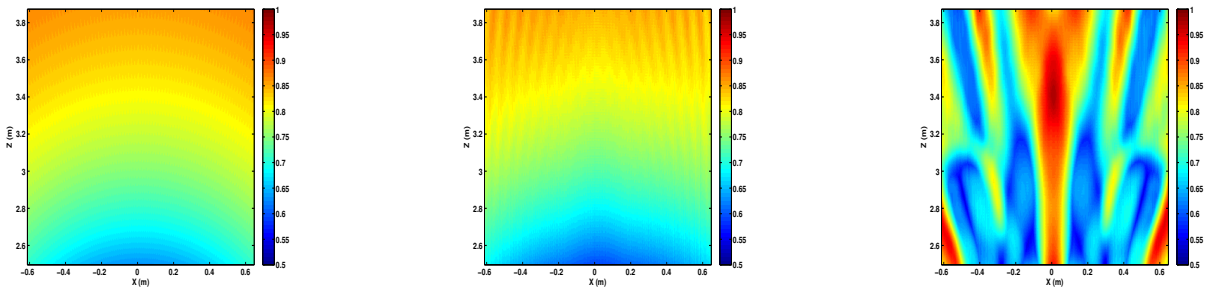

Fig. 4. Magnitude of the peak of array processing results using (a) ground truth data and FDTD simulation data for (b) multilayered brick wall and (c) reinforced concrete wall.

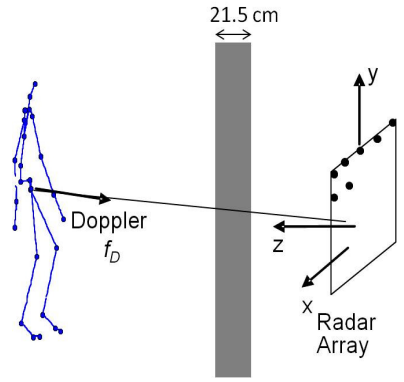

Fig. 5. Frontal imaging of a human through a wall with Doppler processing and compressed sensing based beamforming

r_1 and r_2 are the distances between the point scatterer and the transmitting and receiving antenna elements respectively and k is the propagation constant corresponding to 7.5GHz.

A. Radar Imaging Using Array Processing with 400 Antenna Elements

When the human is moving, the torso and limbs move at different radial velocities with respect to the radar. Therefore, we resolve the body parts on the basis of their micro-Dopplers through Fourier processing along the time domain. Subsequently, the azimuth and elevation of each point scatterer of the human body are estimated through two-dimensional beamforming. Therefore, the multiple point scatterers are now resolved in three dimensions - Doppler, azimuth and elevation. The incorporation of the additional Doppler dimension enables us to relax the resolution requirements along the azimuth and elevation dimensions. The peak scatterers for each Doppler are convolved with point spread response functions along the azimuth-elevation dimensions and summed to obtain the Doppler-enhanced frontal radar images of the humans. This algorithm is presented in greater detail in [11]. Detailed studies in [11] established that we are able to generate high resolution images of humans, in free space, with a continuous wave Doppler radar operating at 7.5 GHz with a uniform planar aperture with $[20 \times 20]$ elements.

Fig.6(a) shows the frontal radar image of a human at a distance of 3m from the radar aperture in free space conditions. This image is generated from the ground truth free space radar data. The sampling frequency of the data is 500Hz. Doppler processing is carried out over a 0.5s time interval. In this image, we can identify both arms and legs of the human. We compare this image with Fig.6(b), the radar image of the human behind the multilayered brick wall. This differs from the previous result in the following ways - First, the strength of the radar signals have been attenuated by two-way propagation through the wall; Second, the positions of some of the point scatterers have been shifted in the azimuth axis due to refraction of signal through the wall. There is no similar shift in the position along the elevation since the wall has been assumed to be uniform along the Y axis. The normalized root mean square (RMS) error between the two images is close to 10%. Finally, we consider the radar image of the human behind the reinforced concrete wall as shown in Fig.6(c). Though the image is distorted, we can still discern the contours of the human. The right arm and leg are clear in the image while the left arm and leg are not. This is because the point scatterers corresponding to the left arm and leg lie in those regions where the radar signal is weak due to destructive interference between the multipath components. The normalized RMS error between this image and the ground truth image is close to 12%

B. Radar Imaging Using Compressed Sensing with 100 Antenna Elements

The results presented in Fig.6 were generated with a planar array with 400 elements. In [11], we demonstrated that it is possible to generate high resolution radar images with sub-Nyquist number of antenna elements by incorporating compressed sensing (CS) principles into two-dimensional beamforming. In free space conditions, CS enabled us to image humans with just 100 antenna elements without significant deterioration in the radar image quality. The technique was robust up to a signal to noise ratio of 10dB. Now, we test the robustness of the technique to wall propagation effects. Fig.7 shows the radar images of humans generated with only 25% of the total number of elements of the $[20 \times 20]$ planar array. First, we consider the radar image of the ground truth free space data in Fig.7(a). When compared to Fig.6(a), the image quality has not significantly deteriorated. The normalized RMS error between the two images is below 2.5% despite 75% reduction in the number of antenna elements. Next, we con-

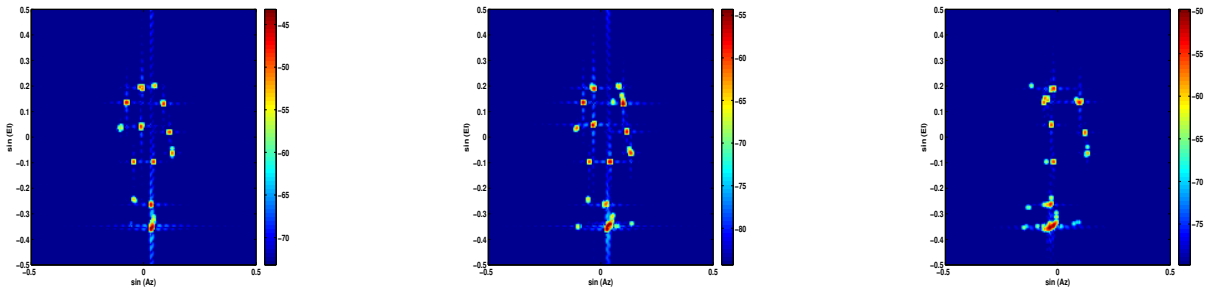

(a) (b) (c)

Fig. 6. Doppler-enhanced frontal image of human using array processing with 400 antenna elements for (a) ground truth data and FDTD simulation data for (b) multilayered brick wall and (c) reinforced concrete wall.

sider the radar images generated from through-wall scenarios. For the multilayered brick wall case, the image quality has not significantly deteriorated and the RMS error introduced by compressed sensing is less than 12.5%. We can identify both arms and legs as well as the torso of the human. In the inhomogeneous wall case, the error is higher and it is difficult to discern the left arm and leg.

In order to quantify the error introduced by radar imaging with sub-Nyquist sampling, we calculate the RMS error between the CS based image and the ground truth image generated from array processing of data from 400 elements. $CS(\%)$ indicates the degree of compression or the percentage of the number of antenna elements of the $[20 \times 20]$ array that were used for imaging. In order to remove the impact of the attenuation introduced by the walls on the radar signals, all the images are normalized to a peak strength of 0dBm before the error is computed. The results are presented in Fig.8. The results show that as the degree of compression increases i.e. as the number of antenna elements are reduced, the RMS error increases only marginally. Therefore, CS offers real benefit in terms of reduced complexity without introducing significant error. The results also show that the error is highest for the reinforced concrete wall case followed by the multilayered brick wall case followed by the free space case. This is consistent with the results presented earlier in Section III. Therefore, the main component of error arises from the multipath introduced by inhomogeneous walls rather than sub-Nyquist sampling while radar imaging.

V. Conclusion

This work examines the effects of wall propagation phenomena on Doppler-enhanced frontal radar imaging of humans. Frontal imaging is realized by combining micro-Doppler processing with compressed sensing based two-dimensional beamforming in the cross-range dimensions. Homogeneous walls introduce refraction and attenuation of the radar signal but do not significantly distort the radar images of humans. Inhomogeneous walls, on the other hand, introduce spurious artifacts in the radar image as well as error in the direction-of-arrival estimation. In both cases, compressed sensing based radar imaging enable us to use radars of reduced cost and complexity to generate high resolution images.

Acknowledgment

This work is supported by the DST Inspire Fellowship Award by the Government of India.

References

[1] M. G. Amin, *Through-the-wall radar imaging*. CRC press, 2011.
[2] F. Ahmad, M. G. Amin, and S. A. Kassam, "A beamforming approach to stepped-frequency synthetic aperture through-the-wall radar imaging," in *Computational Advances in Multi-Sensor Adaptive Processing, 2005 1st IEEE International Workshop on*. IEEE, 2005, pp. 24–27.
[3] A. Lin and H. Ling, "Doppler and direction-of-arrival (ddoa) radar for multiple-mover sensing," *IEEE transactions on aerospace and electronic systems*, vol. 43, no. 4, pp. 1496–1509, 2007.
[4] R. M. Narayanan, "Through-wall radar imaging using uwb noise waveforms," *Journal of the Franklin Institute*, vol. 345, no. 6, pp. 659–678, 2008.
[5] J. Sachs, M. Aftanas, S. Crabbe, M. Drutarovsky, R. Klukas, D. Kocur, T. Nguyen, P. Peyerl, J. Rovnakova, and E. Zaikov, "Detection and tracking of moving or trapped people hidden by obstacles using ultra-wideband pseudo-noise radar," in *Radar Conference, 2008. EuRAD 2008. European*. IEEE, 2008, pp. 408–411.
[6] N. Maaref, P. Millot, C. Pichot, and O. Picon, "A study of uwb fm-cw radar for the detection of human beings in motion inside a building," *Geoscience and Remote Sensing, IEEE Transactions on*, vol. 47, no. 5, pp. 1297–1300, 2009.
[7] V. Chen, G. Smith, K. Woodbridge, and C. Baker, *Through-the-wall radar imaging*. CRC press, 2010, no. 15.
[8] F. Ahmad and M. G. Amin, "Through-the-wall human motion indication using sparsity-driven change detection," *Geoscience and Remote Sensing, IEEE Transactions on*, vol. 51, no. 2, pp. 881–890, 2013.
[9] A. Yarovoy, L. Ligthart, J. Matuzas, and B. Levitas, "Uwb radar for human being detection," *Aerospace and Electronic Systems Magazine, IEEE*, vol. 21, no. 3, pp. 10–14, 2006.
[10] D. R. Wehner, "High resolution radar," *Norwood, MA, Artech House, Inc., 1987, 484 p.*, vol. 1, 1987.
[11] S. S. Ram and A. Majumdar, "High resolution radar imaging of moving humans using doppler processing and compressed sensing," *Aerospace and Electronic Systems, IEEE Transactions on*, vol. 51, no. 2, pp. 1279–1287, 2015.
[12] Y.-S. Yoon and M. G. Amin, "Compressed sensing technique for high-resolution radar imaging," in *SPIE Defense and Security Symposium*. International Society for Optics and Photonics, 2008, pp. 69 681A–69 681A.
[13] M. A. Herman and T. Strohmer, "High-resolution radar via compressed sensing," *Signal Processing, IEEE Transactions on*, vol. 57, no. 6, pp. 2275–2284, 2009.
[14] L. C. Potter, E. Ertin, J. T. Parker, and M. Cetin, "Sparsity and compressed sensing in radar imaging," *Proceedings of the IEEE*, vol. 98, no. 6, pp. 1006–1020, 2010.
[15] V. M. Patel, G. R. Easley, D. M. Healy Jr, and R. Chellappa, "Compressed synthetic aperture radar," *Selected Topics in Signal Processing, IEEE Journal of*, vol. 4, no. 2, pp. 244–254, 2010.
[16] S.-J. Wei, X.-L. Zhang, J. Shi, and G. Xiang, "Sparse reconstruction for sar imaging based on compressed sensing," *Progress In Electromagnetics Research*, vol. 109, pp. 63–81, 2010.

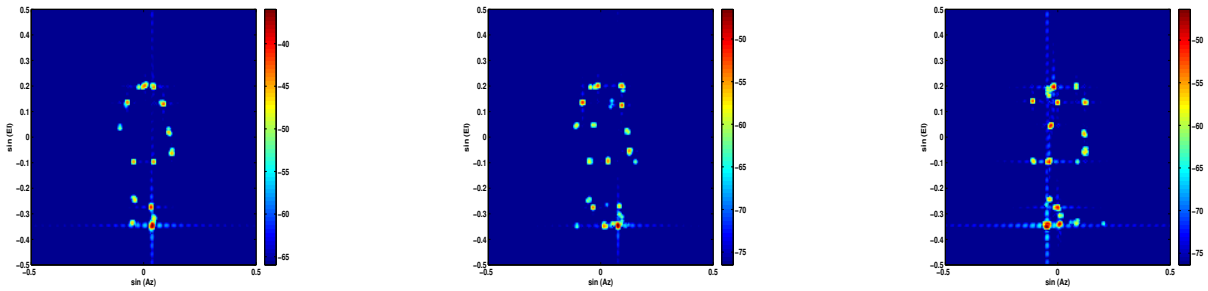

(a) (b) (c)

Fig. 7. Doppler-enhanced frontal image of human using compressed sensing with 100 antenna elements for (a) ground truth data and FDTD simulation data for (b) multilayered brick wall and (c) reinforced concrete wall.

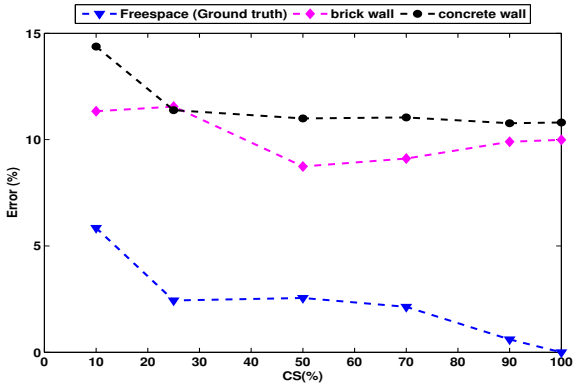

Fig. 8. Normalized RMS error between CS based radar images, generated with sub-Nyquist number of antenna elements in the planar array, and ground truth image, for free space and through-wall scenarios.

[17] S.-J. Wei, X.-L. Zhang, and J. Shi, "Linear array sar imaging via compressed sensing." *Progress In Electromagnetics Research*, vol. 117, 2011.

[18] E. Aguilera, M. Nannini, and A. Reigber, "Multisignal compressed sensing for polarimetric sar tomography," *Geoscience and Remote Sensing Letters, IEEE*, vol. 9, no. 5, pp. 871–875, 2012.

[19] ——, "Wavelet-based compressed sensing for sar tomography of forested areas," in *Synthetic Aperture Radar, 2012. EUSAR. 9th European Conference on*. VDE, 2012, pp. 259–262.

[20] ——, "A data-adaptive compressed sensing approach to polarimetric sar tomography of forested areas," *Geoscience and Remote Sensing Letters, IEEE*, vol. 10, no. 3, pp. 543–547, 2013.

[21] J. Fang, Z. Xu, B. Zhang, W. Hong, and Y. Wu, "Fast compressed sensing sar imaging based on approximated observation," *Selected Topics in Applied Earth Observations and Remote Sensing, IEEE Journal of*, 2013.

[22] J. Yang, J. Thompson, X. Huang, T. Jin, and Z. Zhou, "Random-frequency sar imaging based on compressed sensing," *Geoscience and Remote Sensing, IEEE Transactions on*, vol. 51, no. 2, pp. 983–994, 2013.

[23] Q. Huang, L. Qu, B. Wu, and G. Fang, "Uwb through-wall imaging based on compressive sensing," *Geoscience and Remote Sensing, IEEE Transactions on*, vol. 48, no. 3, pp. 1408–1415, 2010.

[24] A. C. Fannjiang, T. Strohmer, and P. Yan, "Compressed remote sensing of sparse objects," *SIAM Journal on Imaging Sciences*, vol. 3, no. 3, pp. 595–618, 2010.

[25] S. Gogineni and A. Nehorai, "Target estimation using sparse modeling for distributed mimo radar," *Signal Processing, IEEE Transactions on*, vol. 59, no. 11, pp. 5315–5325, 2011.

[26] Y. Yu, A. P. Petropulu, and H. V. Poor, "Mimo radar using compressive sampling," *Selected Topics in Signal Processing, IEEE Journal of*, vol. 4, no. 1, pp. 146–163, 2010.

[27] S. S. Ram, C. Christianson, Y. Kim, and H. Ling, "Simulation and analysis of human micro-dopplers in through-wall environments," *Geoscience and Remote Sensing, IEEE Transactions on*, vol. 48, no. 4, pp. 2015–2023, 2010.

[28] D. M. Sullivan, *Electromagnetic simulation using the FDTD method*. John Wiley & Sons, 2013.